Investigation of Turbulent Dense Gas Flows with Direct Numerical Simulation

A. Vadrot[a], A. Giauque[a], C.Corre[a]

a. LMFA - Laboratoire de Mécanique des Fluides et d'Acoustique
Ecole Centrale de Lyon, 36 avenue Guy de Collongue, 69134 Ecully Cedex, France
alexis.giauque@ec-lyon.fr

Résumé

Le projet de recherche EDGES (ANR 2018–2022) est consacré à l'analyse et à la modélisation de la turbulence dans les écoulements de gaz denses, qui sont d'un intérêt majeur pour la communauté industrielle active en récupération et transfert de la chaleur. Pour identifier les éventuelles caractéristiques spécifiques de la turbulence induites par les propriétés thermodynamiques atypiques des gaz denses, une base de données de type Simulation Numérique Directe (SND) est produite pour deux configurations académiques : turbulence homogène isotrope (THI) forcée et couche de mélange compressible. Le spectre de l'énergie cinétique turbulente calculé pour le cas de THI forcée est proche de celui obtenu dans le cas incompressible, même lorsque le nombre de Mach turbulent est élevé. La réduction de la dissipation compressible d'énergie cinétique turbulente peut être reliée au découplage des fluctuations de masse volumique et de vitesse ainsi qu'à l'atténuation des shocklets de compression dans le gaz dense. Le cas de la couche de mélange compressible à Mach convectif $M_c = 1.1$ montre que la réduction du taux de croissance de l'épaisseur de quantité de mouvement classiquement induite par les effets de compressibilité est faiblement influencée par l'équation d'état du gaz pendant la phase d'auto-similarité. La croissance instable conduisant à cette phase auto-similaire est en revanche fortement amplifiée par la thermodynamique du gaz dense.

Abstract

The EDGES research project (ANR 2018–2022) is devoted to the analysis and modeling of turbulence in dense gas flows. Dense gases are of primary interest to the industrial community working on heat recovery and transfer. In order to identify the potential specificies of turbulence characteristics for dense gas flows induced by their pecular thermodynamic properties, a Direct Numerical Simulation (DNS) database is produced for two academic configurations : forced homogeneous isotropic turbulence (HIT) and compressible mixing layer. The statistically stationary turbulent kinetic energy (TKE) spectrum computed for HIT follows quite closely the one obtained in the incompressible case even when the turbulent Mach number is large. The weakening of compressible dissipation of the TKE can be related to the decoupling of density and velocity fluctuations as well as to the strong weakening of compression shocklets in the dense gas. The mixing layer case at a convective Mach number $M_c = 1.1$ shows that the well-known compressibility-related reduction of the momentum thickness growth rate is only very slightly influenced by the Equation of State during the self-similar stage. The unstable growth leading to the self-similarity phase is however greatly enhanced by the dense gas thermodynamics.

Mots-clés : Turbulence; SND; gaz dense; THI; couche de mélange

Keywords : Turbulence; DNS; dense gas; HIT; Mixing layer

1 Introduction

The goals of the ANR EDGES research project (2018–2022) are the analysis and modeling of turbulence in dense gas flows, with a subsequent transfer of this fundamental knowledge to the application field of Organic Rankine Cycle turbine modeling where dense gases are commonly used as working fluids because of their peculiar thermodynamic properties. The key steps of the project are : 1) build a database of turbulent dense gas flows using Direct Numerical Simulation (DNS); 2) perform an *a priori* assessment of current LES and RANS closure models; 3) propose, if needed, new LES and RANS models for dense gas flows and 4) perform an *a posteriori* assessment of the relevance of these new closure models for a full ORC turbine stage. The present contribution reports some preliminary results obtained in the first step of the project, which corresponds to the analysis of a DNS database for two academic configurations : forced homogeneous isotropic turbulence (HIT) and compressible mixing layer. The DNS methodology is briefly described in section 2. Key findings for the HIT configuration and the mixing layer case are reported in section 3, with an emphasis on the differences / similarities found in the structure of turbulence between the perfect gas and the dense gas flows (in particular occurrence of shocklets for HIT, time evolution of the momentum thickness for the mixing layer, turbulent kinetic energy and velocity power spectrum analysis).

2 Direct Numerical Simulation methodology

2.1 Numerical solver

DNS are performed thanks to the unstructured numerical solver AVBP [1]. The code solves the full compressible Navier-Stokes equations using a two-step time-explicit Taylor-Galerkin scheme for the hyperbolic terms expressed in a cell-vertex formulation [2]. The TTGC and TTG4A schemes provide third-order accuracy in space and respectively third-order or fourth-order accuracy in time [2]. To preserve the positivity of the solution in regions where very strong gradients exist, a hyperviscosity β is introduced in the viscous stress tensor τ_{ij}, following the approach of Cook and Cabot [3] .

2.2 Equation of State (EoS) and transport coefficients

The dense gas considered in this study is FC-70[4], whose thermodynamic behavior close to the critical point is accurately described using the EoS proposed by Martin and Hou [5]. Transport properties are described using the model developed by Chung *et al.*[6]. When needed and for comparison purposes, the perfect gas EoS is used in combination with Sutherland model to describe the evolution of molecular viscosity with temperature and the Prandtl number is set equal to 0.71 to determine the heat conductivity.

2.3 Turbulence forcing methodology

A forcing methodology is applied to the HIT flow in order to reach statistical stationarity. Because the numerical tool used for this research project is a temporal DNS solver, the linear forcing model initially proposed by Lundgren [7] and studied by Rosales and Meneveau [8] is adopted. The linear forcing scheme for incompressible turbulence has been since analyzed in the compressible context by Petersen

and Livescu [9] and is similar to the natural Reynolds shear stress production mechanism in the TKE equation.

3 A DNS database of turbulent dense gas flows

3.1 Forced HIT

The key characteristics of the five DNS computations performed in this study are summarized in table 1. The initial Taylor Reynolds number is set to 100 for all simulations which are initialized using an incompressible homogeneous isotropic turbulent velocity field following the Passot-Pouquet spectrum with k_e the wavelength of the maximum initial kinetic energy defined by the relationship $Re_\lambda = \sqrt{15 * 2\pi u_{rms}/(\nu k_e)}$. Because of the low speed of sound obtained using the Martin & Hou (MH) EoS for the chosen thermodynamic point, a 20 m/s turbulent velocity translates into a turbulent Mach number equal to 0.8. For computations using the perfect gas (PG) EoS, a 63 m/s turbulent velocity is imposed in order to reach the same turbulent Mach number.

Table 1: Characteristics of the DNS test cases (Forced HIT)

Case name	EoS	Mesh size (number of cells)	Turbulent velocity (m/s)	Turbulent Mach Number	Initial Taylor Re number
MH1	Martin & Hou	540^3	20	0.8	100
MH2	Martin & Hou	675^3	20	0.8	100
MH3	Martin & Hou	800^3	20	0.8	100
PG1	Perfect gas	540^3	63	0.8	100
PG2	Perfect gas	675^3	63	0.8	100

Given the common initial Taylor Reynolds number, the 540^3, 675^3 and 800^3 resolutions correspond to a discretization of the Kolmogorov length scale with respectively 2, 2.5 and 3 points. Figure 1 displays the temporal evolution of the kinetic energy and enstrophy for the dense gas. Both quantities are normalized by their initial value and the time is normalized by the characteristic turn-over time defined as $\tau_0 = L_i/u_{rms}$. It is observed computations MH2 and MH3 provide a very close evolution both for the kinetic energy and for the enstrophy even though this last quantity is of a higher order. This result is consistent with the fact that the Kolmogorov length scale does not need to be perfectly discretized in order to achieve an accurate prediction because only a very small fraction of the kinetic energy remains at this scale [10].

Comparison of perfect and dense gas TKE spectra

When studying largely compressible Euler turbulence, Kritsuk *et al.* [11] show that Kolmogorov's cascade phenomenology, which leads to the well known $-5/3$ decay of the TKE spectrum with the wavenumber, has to be corrected to take into account compressibility. They show that the velocity power spectrum defined as $< \widehat{u_i^2} >/2$ follows a -2 slope for a significantly compressible flow while the TKE spectrum defined as $< \widehat{\left(\sqrt{\rho}u_i\right)^2} > /2$ follows a $-3/2$ slope. It can be inferred that, as the turbulent Mach number increases, the departure between the velocity power and the TKE spectra reflects the influence of compressibility on turbulence.

Figure 2 compares the velocity power spectrum and the TKE spectrum obtained in case MH2 and PG2 at $t = 15\tau$ using respectively the MH EoS and the PG EoS. In order to remove forcing-related effects from the comparison, all spectra are normalized by their value for $k = 4k_{min}$.

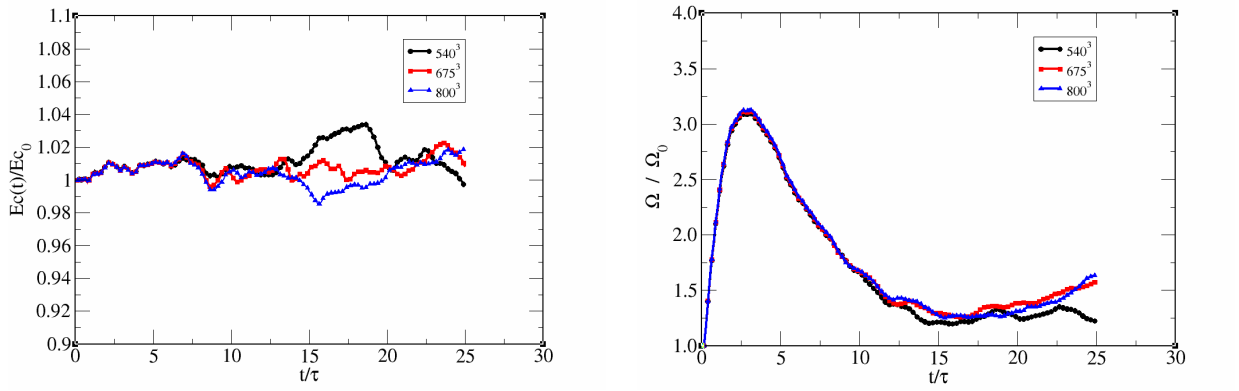

Figure 1: Evolution of the normalized kinetic energy (left) and normalized enstrophy (right) with time for cases MH1, MH2 and MH3.

The inertial range is restricted to a narrow region in the spectral space between $k = 4k_{min}$ and $k = 20k_{min}$. This is believed to be due to the moderate Taylor Reynolds number reached in the presented cases. Figure 2 therefore also features a closer view focused on the inertial range. In this region, the velocity power spectrum obtained with the MH EoS departs only slightly from the TKE spectrum. Thus, compressibility effects in the dense gas flow have a reduced influence on the flow turbulence with respect to the perfect gas case. Additionally, the slope of both velocity power and TKE spectra takes a value close to $-5/3$ in the inertial range, which corresponds to the incompressible scaling although the turbulent Mach number is 0.8. As far as the perfect gas is concerned, the spectra followed by velocity power and TKE are more significantly separated from each other as expected. Yet, if the velocity power spectrum slope is close to the expected -2 slope, the TKE spectrum does not follow the expected $-3/2$ slope. The key observation made at this stage is that, for the studied Taylor Reynolds number, compressibility does not significantly affect the turbulence cascade in the dense gas flow, even at a fairly large turbulent Mach number.

The dissipation region close to the Kolmogorov wavenumber (beyond $k = 100k_0$) reveals another interesting difference between the turbulent flows modeled using either PG or MH EoS. A much larger dissipation of both the velocity power and the TKE is observed in the perfect gas case. This difference between perfect and dense gas is believed to be due, at least in part, to the departure in the shocklets behavior between the two types of flows, as described in the next section.

Shocklets analysis

To analyze shocklets in the compressible configuration under study the marching cube algorithm proposed by Samtaney *et al.* [12] is implemented. The iso-surfaces of zero density Laplacian ($\Delta\rho = 0$) are first detected in the flow. Next, in order to only keep iso-surfaces corresponding to actual shocklets, the generalized Rankine-Hugoniot condition across the shocklet:

$$2(h_2 - h_1) = (p_2 - p_1)\left(\frac{1}{\rho_1} + \frac{1}{\rho_2}\right) \tag{1}$$

is verified between left and right states, with a distance set to $4\Delta x$ in the direction normal to the discontinuity since it is known from previous studies [13] that the shock is typically spread over four cells with the numerical solver in use. Jumps verifying the relation within 10% of the mean enthalpy are flagged

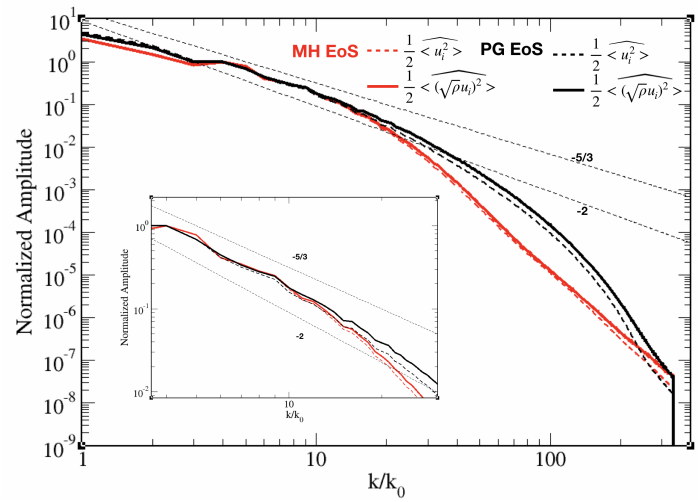

Figure 2: Comparison of TKE and velocity power spectra at $t = 15\tau$ as a function of the EoS.

as Eq (1) is only strictly valid in the inviscid context. Note the generalized Rankine-Hugoniot relation retains its validity regardless of the velocity of the shocklet itself, which could be complex to compute. When describing FC-70 as a perfect gas, the value of γ is very close to unity, so that the density and pressure jumps are expected to be almost the same. Figure 3 displays the distribution of the density and entropy jumps as a function of the pressure jump across shocklets in case PG2. It confirms that $\rho_2/\rho_1 \approx p_2/p_1$. Figure 3 also shows that very strong compression shocklets are observed in case PG2 up to $\rho_2/\rho_1 = 45$. It can also be observed the entropy increase through the compression shocklet follows quite closely Rankine-Hugoniot theory leading to strong entropy jumps as the pressure ratio through the shocklet increases.

Compression shocklets are also observed in the dense gas case (MH2) which are shown in Fig. 4. The dissipative structures observed at $t = 15\tau$ are intricate and form a dense net. At the center of each structure, the divergence of the velocity is strongly negative which corresponds to the focal point of compression : values as large as ten times the average velocity divergence are observed.

When applying the detection algorithm in search of expansion shocklets, none have been found in the perfect gas case as expected. In the dense gas case however, some structures are identified that correspond to expansion shocklets, as displayed in Fig. 5.

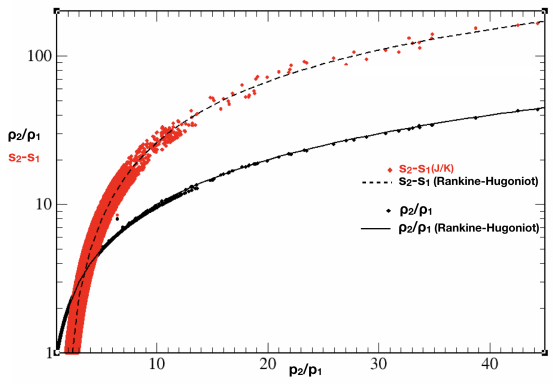

Figure 3: Compression shocklets density jump and entropy increase as a function of the pressure jump for case PG2 at $t = 15\tau$.

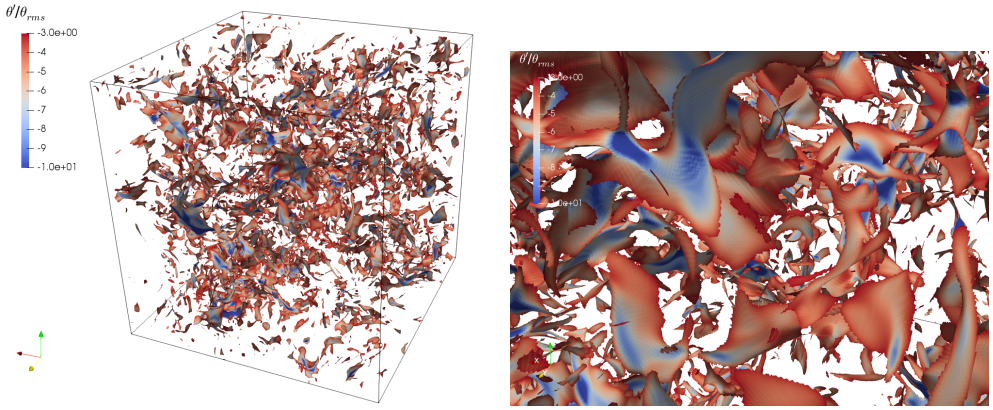

Figure 4: Forced HIT (MH2 at $t = 15\tau$). Visualization of compression shocklets colored by the contours of the local velocity divergence normalized by the average velocity divergence over the flow domain (range of variation $[-10, -3]$).

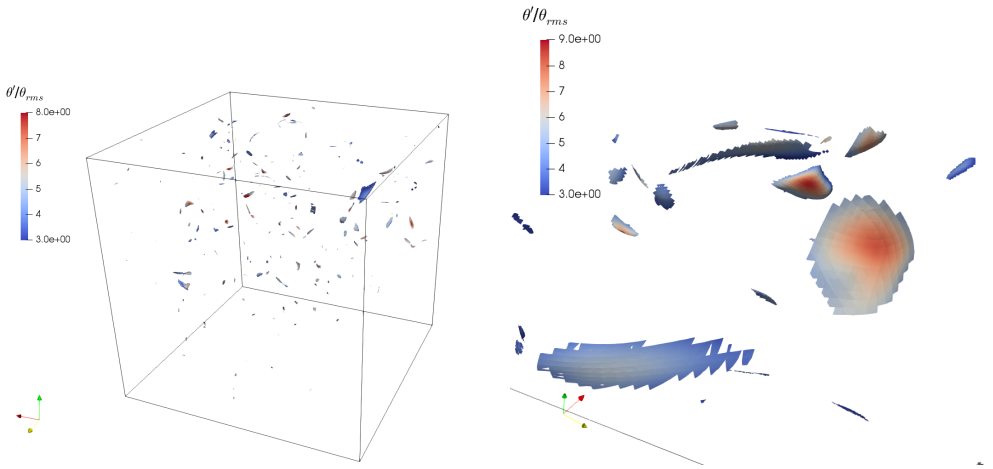

Figure 5: Forced HIT (MH2 at $t = 15\tau$). Visualization of expansion shocklets colored by the contours of the local velocity divergence normalized by the average velocity divergence over the flow domain (range of variation $[+3, +8]$).

3.2 Mixing Layer

The DNS of a temporal shear layer is performed for the flow configuration described in Figure 6 : the two streams flow in opposite directions, enabling to increase the differential velocity with a lesser magnitude for each stream velocity. Periodic boundary conditions are applied in the x and z directions while non-reflecting boundary conditions are applied in the y direction.

Following the reference PG simulation of Pantano & Sarkar [14], the convective Mach number is set equal to 1.1 and the values provided in Table 2 are chosen for the simulations. The ratio r between the Kolmogorov scale and the cell size is about 0.39 for the least refined mesh (16.8M simulation). Since this ratio can be considered as not very large for a DNS, a second DNS has been performed with a refined

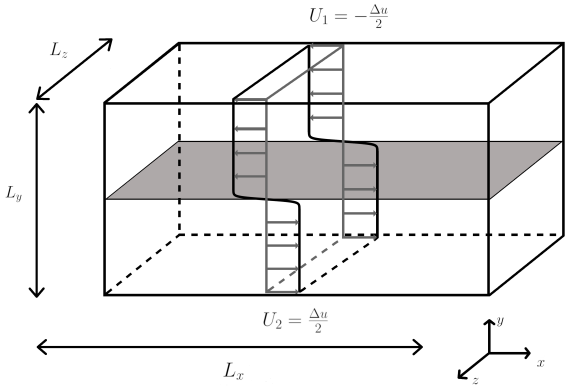

Figure 6: Schematic of the shear layer configuration. The grey plane represents the initial momentum thickness and its thickness is at scale with the lengths of the computational domain.

mesh obtained by doubling the number of grid cells in each direction (134M simulation) yielding a ratio r equal to 0.78.

Temporal evolution of the momentum thickness

The computation of the TKE balance requires to define the self-similar range where the mixing layer growth rate evolves linearly with time. The time evolution of turbulent quantities is therefore investigated to identify the self-similar range of the compressible shear layer under stuy. The momentum thickness temporal evolution is drawn in Figure 7a) for both the PG and MH EoS. The curves are initially very close, with a different evolution for perfect and dense gas mixing layer taking place in the second step of the mixing layer development, when the unstable growth is governed by instability modes. The MH unstable growth is faster than the PG one, likely because instability modes and their amplification factor evolve differently for PG and MH mixing layers. Vreman *et al.* [15] have shown that the mixing layer momentum thickness growth rate is proportional to the integrated production term. Figure 7b) displays the production term integrated over the whole domain for MH and PG calculations : the integrated MH term is found to be larger than the integrated PG term, consistently with the MH/PG momentum thickness evolution. The time period defining the self-similar stage is indicated in Figure 7b). Although the unstable evolution is faster for the MH shear layer, both MH and PG shear layers reach a self-similar stage almost at the same time as confirmed by Figure 7b). The growth rate slopes calculated during the self-similar stage are reported in Figure 7a) : the slope is slightly larger for the MH than for the PG with a typical 5% difference between PG and MH shear layers.

Table 2: Simulation parameters for the mixing layer case. L_x, L_y and L_z are domain lengths normalized by the initial momentum thickness $\delta_{\theta,0}$. N_x, N_y and N_z denote the number of grid points in each space direction.

	M_c	ρ_1/ρ_2	$Re_{\delta_{\theta,0}}$	$L_x \times L_y \times L_z$	$N_x \times N_y \times N_z$	$\Delta u\ (m.s^{-1})$	$\delta_{\theta,0}\ (nm)$
Air	1.1	1.0	160	$344 \times 172 \times 86$	$512 \times 256 \times 128$	375.18	12.348
Air	1.1	1.0	160	$344 \times 172 \times 86$	$1024 \times 512 \times 256$	375.18	12.348
FC-70	1.1	1.0	160	$344 \times 172 \times 86$	$512 \times 256 \times 128$	62.3183	188.18
FC-70	1.1	1.0	160	$344 \times 172 \times 86$	$1024 \times 512 \times 256$	62.3183	188.18

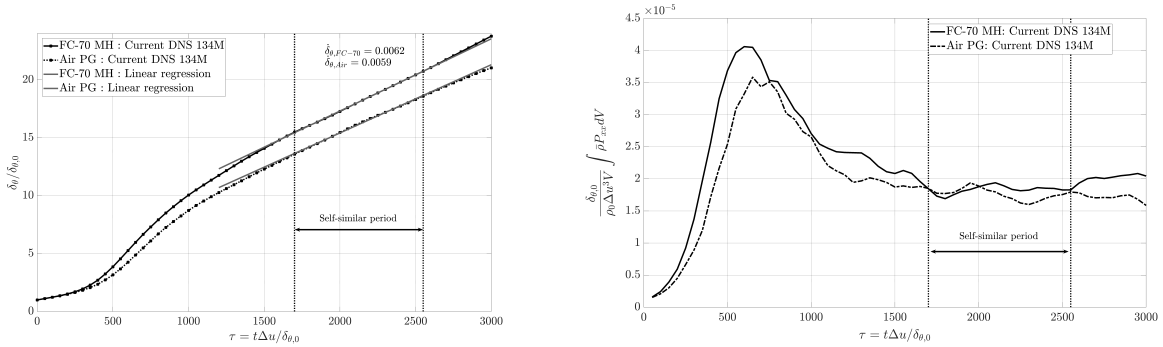

a) b)

Figure 7: Comparison between MH (Martin-Hou EoS) and PG (Perfect Gas EoS). a) Temporal evolution of the mixing layer momentum thickness. b) Temporal evolution of the normalized integrated production.

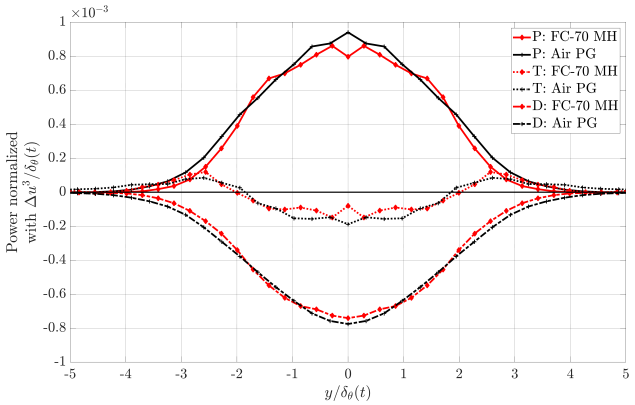

Figure 8: Comparison between MH and PG mixing layers. Evolution of the normalized power quantities over the y direction. P: Production, D: Dissipation and T: Transport are normalized by $\Delta u^3/\delta_\theta(t)$.

Turbulent kinetic energy (TKE) balance

The previously identified self-similar stages are appropriate to study the TKE equation. Figure 8 displays the comparison of the TKE budget terms between the MH and the PG mixing layers. The dense gas effects seem to have a very limited impact on these integrated quantities during the self-similar stage. However, a noticeable effect induced by the dense gas is the slower propagation of the turbulent terms at the boundaries of the mixing layer. The other terms of the TKE equation - the compressible dissipation, the pressure-dilatation, the mass-flux coupling term and the convective derivative of the TKE - are negligible. Residuals and the time derivative of the TKE are not represented for clarity reasons, but agree perfectly between both gases. The pressure-strain terms are not negligible, but no significant difference is observed between MH and PG.

Spectrum of the turbulent kinetic energy (TKE)

Since a key objective of the research project is to assess the need for new LES sub-grid models in the case of turbulent dense gas flows, it is required to have a closer look at each quantity in the spectral domain. The TKE streamwise spectra are plotted in Figure 9a) for PG and MH mixing layers. Spectra are normalized by $\Delta u^2 \delta_\theta(t)$. The evolution of TKE at the largest scales is similar for both gases. However,

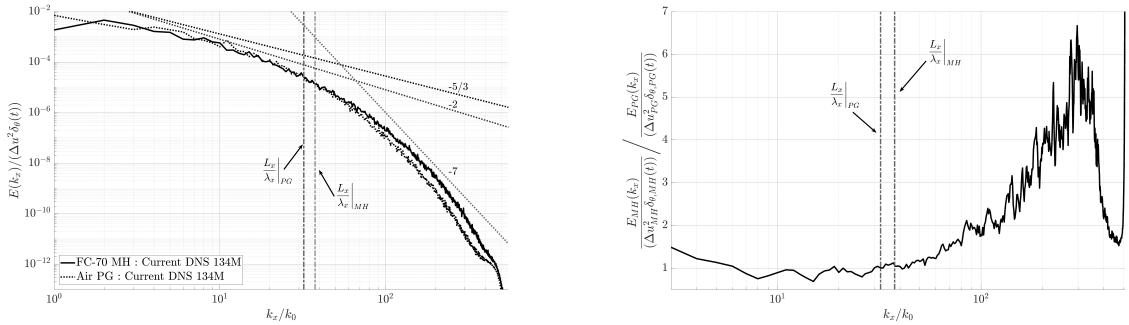

Figure 9: Comparison between MH and PG mixing layers. a) Streamwise spectra. b) MH / PG streamwise spectra ratio.

at small scales, the PG TKE is decreasing faster than the MH TKE. The dense gas effect seems therefore to increase small scales energy. This result is consistent with preliminary conclusions arising from the previous analysis of the forced HIT. Figure 9b) displaying the MH/PG spectra ratio precisely identifies the quantities at stake : at scales smaller than the Taylor microscale, the MH to PG energy ratio increases up to a factor of six.

4 Concluding remarks

Preliminary results obtained in the framework of the ANR research project EDGES have been presented to provide insight into the characteristics of dense gas turbulent flows with respect to perfect gas turbulent flows. The analysis of turbulence in the forced HIT configuration shows that compressibility effects are almost suppressed in the dense gas as the correlation of velocity and density fluctuations is significantly reduced by the complex thermodynamics. Interestingly, the compressible mixing layer configuration indicates that during the self-similar regime, the momentum thickness growth rate is almost the same for perfect gas and dense gas modeled using Martin-Hou EoS. These contrasted preliminary conclusions clearly support the choice made in the project to ground the analysis and modeling of turbulence in dense gas flows on DNS of various flow configurations and also call for further investigation : ongoing work includes in particular shear layer DNS for larger values of the convective Mach number also leading to larger values of the turbulent Mach number.

5 Acknowledgements

This work is supported by the JCJC ANR EDGES project, grant #ANR-17-CE06-0014-01 of the French Agence Nationale de la Recherche. Simulations have been carried out using HPC ressources at CINES under the project grant #A0042A07564. Some of the results detailed in this article have been presented at the second International Seminar on Non-Ideal Compressible-Fluid Dynamics held at Bochum, Germany in October 2018.

References

[1] Thilo Schönfeld and Michael Rudgyard. Steady and Unsteady Flow Simulations Using the Hybrid Flow Solver AVBP. *AIAA Journal*, 37(11):1378–1385, nov 1999.

[2] Olivier Colin and Michael Rudgyard. Development of High-Order Taylor–Galerkin Schemes for LES. *Journal of Computational Physics*, 162(2):338–371, aug 2000.

[3] Andrew W. Cook and William H. Cabot. A high-wavenumber viscosity for high-resolution numerical methods. *Journal of Computational Physics*, 195(2):594–601, apr 2004.

[4] Alberto Guardone and B M Argrow. Nonclassical gasdynamic region of selected fluorocarbons. *Physics of Fluids*, 17(11):1–17, 2005.

[5] Joseph J Martin and Yu-chun Hou. Development of an Equation of State for Gases. *AIChE journal*, 2(4):142–151, 1955.

[6] Ting Horng Chung, Mohammad Ajlan, Lloyd L. Lee, and Kenneth E. Starling. Generalized multiparameter correlation for nonpolar and polar fluid transport properties. *Industrial & Engineering Chemistry Research*, 27(4):671–679, apr 1988.

[7] T. S. Lundgren. Linearly forced isotropic turbulence. *Annual Research Briefs*, (2):461–473, 2003.

[8] Carlos Rosales and Charles Meneveau. Linear forcing in numerical simulations of isotropic turbulence: Physical space Implementations and convergence properties. *Physics of Fluids*, 17(9):1–8, 2005.

[9] Mark R. Petersen and Daniel Livescu. Forcing for statistically stationary compressible isotropic turbulence. *Physics of Fluids*, 22(11), 2010.

[10] Parviz Moin and Krishnan Mahesh. Direct numerical simulation: A tool in turbulence research. *Annual Review of Fluid Mechanics*, 30(1):539–578, 1998.

[11] Alexei G. Kritsuk, Michael L. Norman, Paolo Padoan, and Rick Wagner. The Statistics of Supersonic Isothermal Turbulence. *The Astrophysical Journal*, 665(1):416–431, aug 2007.

[12] Ravi Samtaney, D. I. Pullin, Branko Kosović, Branko Kosovic, and I Introduction. Direct numerical simulation of decaying compressible turbulence and shocklet statistics. *Physics of Fluids*, 13(5):1415–1430, 2001.

[13] A Giauque, C Corre, and M Menghetti. Direct numerical simulations of homogeneous isotropic turbulence in a dense gas. *Journal of Physics: Conference Series*, 821(1):12017, 2017.

[14] C. Pantano and S. Sarkar. A study of compressibility effects in the high-speed turbulent shear layer using direct simulation. *Journal of Fluid Mechanics*, 451(2002):329–371, 2002.

[15] Bert Vreman, Bernard Geurts, and Hans Kuerten. Subgrid-modelling in LES of compressible flow. *Applied Scientific Research*, 54(3):191–203, 1995.